Scientia Iranica A (2015) 22(6), 1981–1993

Sharif University of Technology
Scientia Iranica
Transactions A: Civil Engineering
www.scientiairanica.com

Study of thermo-hydro-mechanical response of saturated clayey soils using two thermo-plastic constitutive models

S. Delfan, H. Shahir*, **A. Hamidi and E. Lotfi**

Department of Civil Engineering, Faculty of Engineering, Kharazmi University, Tehran, P.O. Box 15719-14911, Iran.

Received 17 December 2013; received in revised form 24 January 2015; accepted 26 April 2015

KEYWORDS
Thermo-hydro-mechanical response;
Finite element method;
Thermoplastic constitutive model;
Saturated clay;
Thermal consolidation.

Abstract. In this article, Thermo-Hydro-Mechanical (THM) response of saturated clays has been studied. For this purpose, the finite element program PISA, which is able to simulate coupled THM analysis, has been employed. Due to the effects of temperature on the mechanical behavior of soil, two temperature-dependent constitutive models have been implemented in PISA. For verification of the developed numerical model, ATLAS large scale experiment has been simulated in different conditions and the simulations results have been compared with in-situ measurements. Comparison of predictions and measurements reveals that by using coupled formulation along with thermoplastic constitutive models, the main aspects of the THM behavior of saturated clays can be captured. The results indicate that for accurate simulation of advection phenomenon, two-dimensional finite element model should be used.

1. Introduction

The generated heat by a source in the clay formation causes the temperature of soil to increase. As a result of temperature increase in saturated soils, the pore water and soil skeleton are expanded. In general, volume augmentation of the pore water is more than that of the voids in the soil structure. The temperature induced differential volume change will lead to an increase in pore water pressure and consequently effective stress reduction. The dissipation of temperature-induced excess pore water pressure causes volume change in the soil mass. This phenomenon is called thermal consolidation. It is a coupled Thermo-Hydro-Mechanical (THM) phenomenon because of simultaneous occurrence of pore water flow, temperature variation, and solid phase deformation. In recent years, coupled Thermo-Hydro-Mechanical (THM) problem has been a subject of many studies such as geological disposal of radioactive wastes, geothermal energy extraction, thermal removal of soil pollution, and oil and other hydrocarbons extraction.

Several large-scale field heating tests have been carried out at underground research laboratories in some countries. In these experiments, several sensors have been placed at different intervals to measure the variation of temperature, pore water pressure, displacements, and in-situ stresses around the thermal source. A soil heating test was conducted at Kamaishi Mine in Japan [1]. The main objective of this study was to evaluate applicability of the engineered barrier technology. Kamaishi Mine experiment was simulated using four finite element codes for prediction of the coupled thermo-hydro-mechanical responses by Rutqvist et al. [2]. Another large-scale underground heating test was conducted at exploratory studied facilities at Yucca Mountain, Nevada, for studying coupled thermo-

*. *Corresponding author. Fax: +98 21 88830891*
E-mail addresses: Delfan.s@gmail.com (S. Delfan); shahir@khu.ac.ir (H. Shahir); hamidi@khu.ac.ir (A. Hamidi); lotfi.elhame@gmail.com (E. Lotfi)

hydro-mechanical and chemical behavior of fractured rock mass during 4 years [3]. Comparison of field measurements with predictions of four different numerical models was done by Rutqvist et al. [4]. In FEBEX in-situ test which was installed in Grimsel test site in Switzerland, the behavior of crystalline rock as a host formation in deep geological storage was studied [5]. Gens et al. [6] simulated this experiment using finite element code CODE-BRIGHT. HE-D test was conducted in Mont Terri underground laboratory to simulate thermo-hydro-mechanical response of Opalinus clay [7]. In HADES-URF laboratory in MOL, Belgium, several thermo-hydro-mechanical tests were conducted. Admissible Thermal Loading for Argillaceous Storage (ATLAS) is one of these tests, which was done between the years of 1990 to 1994 [8]. This test was designed to investigate the behavior of Boom clay as a host formation in deep geological storages.

In this paper, the coupled formulation governing the Thermo-Hydro-Mechanical phenomenon in saturated porous medium [9] was used to study the behavior of saturated clayey soil mass under thermal loading. For constitutive modeling of clay, two thermo-plastic models proposed by Abuel-Naga et al. [10] and Hamidi and Khazaei [11] were implemented in the finite element program PISA. Then, the developed numerical model was used to simulate the ATLAS experiment in one-dimensional and two-dimensional conditions. The results of simulations of ATLAS experiment using two constitutive models have been compared with in-situ measurements of temperature, pore water pressure, and displacements, in order to verifying the accuracy of different assumptions in THM modeling of saturated clay layers.

2. Formulation of the numerical model

The comprehensive mathematical formulations for Thermo-Hydro-Mechanical (THM) behavior of saturated and partially saturated porous media were presented by Lewis and Schrefler [9]. In this study, water saturated condition was considered and the governing equations were obtained considering the porous medium as a deformable two-phase material (solid matrix and voids fully filled with water). Equations governing the coupled THM process in saturated porous medium consist of momentum balance equation of multi-phase medium, mass balance equation, and energy balance equation, which are briefly presented in the following. Details of these formulations can be found in [9,12].

Linear momentum balance equation in terms of total stress is written as follows:

$$\mathrm{div}\boldsymbol{\sigma} + \rho\mathbf{g} = 0. \tag{1}$$

In this equation, density of two-phase medium is defined as:

$$\rho = (1-n)\rho^s + n\rho^w, \tag{2}$$

where $\mathrm{div}\boldsymbol{\sigma}$ is divergence of total stress tensor, $\mathbf{g}$ the vector of gravitational acceleration in the z-direction, ρ^s the density of solid phase, ρ^w water density, and n soil porosity.

The effective stress is written as follows:

$$\boldsymbol{\sigma} = \boldsymbol{\sigma'} - \alpha\mathbf{I}P^w, \tag{3}$$

where α is Biot's coefficient ($\alpha = 1$ for incompressible grains), $\mathbf{I}$ identity matrix, and P^w macroscopic pressure of pore water. It is notable that tension in the solid phase and compression in the fluid phase are designated with positive sign.

Water flow through saturated porous medium is governed by the Darcy's law as follows:

$$n\mathbf{V}^{ws} = \frac{K}{\mu^w}\left(-\mathbf{grad}P^w + \rho^w\mathbf{g}\right), \tag{4}$$

where $\mathbf{V}^{ws}$ is velocity of water relative to solid phase, K intrinsic permeability, and μ^w dynamic viscosity. The mass balance equation in fully saturated medium is according to the following equation:

$$\left(\frac{\alpha-n}{K_s} + \frac{n}{K_w}\right)\frac{\partial P^w}{\partial t} + \alpha\mathrm{div}\mathbf{V}^s - \beta_{sw}\frac{\partial T}{\partial t} + \frac{K}{\mu^w}\mathrm{div}\left(-\mathbf{grad}P^w + \rho^w\mathbf{g}\right) = 0, \tag{5}$$

where K_s and K_w are bulk modulus of solid and water phases, respectively. t is time and T is temperature. $\beta_{sw} = [(\alpha-n)\beta_s + n\beta_w]$ is effective thermal expansion coefficient of medium, where β_s and β_w are thermal expansion of solid and water phases, respectively.

A constitutive assumption for heat flux is the generalized version of Fourier's law for isotropic media:

$$\mathbf{q} = -\chi_{eff}\mathbf{grad}T, \tag{6}$$

where $\mathbf{q}$ is heat flux and χ_{eff} is effective thermal conductivity based on the following equation:

$$\chi_{eff} = n\lambda_w + (1-n)\lambda_s, \tag{7}$$

where λ_w and λ_s are thermal conductivity of water and solid phases, respectively.

Enthalpy balance equation in this case is of the form:

$$(\rho C_p)_{eff}\frac{\partial T}{\partial t} + \rho^w C_p^w\mathbf{V}^w.\mathbf{grad}T - \mathrm{div}(\chi_{eff}\mathbf{grad}T) = 0, \tag{8}$$

where V^w is velocity of water phase. Effective heat capacity is defined by:

$$(\rho C_p)_{eff} = \rho^s C_p^s + \rho^w C_p^w, \tag{9}$$

where C_p^s and C_p^w are specific heat capacity of solid and water phases, respectively.

Eqs. (1), (5), and (8) are three main governing equations and the independent unknowns in these equations are solid phase displacement $\mathbf{u}$, pore water pressure P^w, and temperature T.

The discretized matrix form of equations is derived by applying the finite element method as follows:

$$\begin{bmatrix} 0 & 0 & 0 \\ 0 & \mathbf{H} & 0 \\ 0 & 0 & \mathbf{K}_t \end{bmatrix} \begin{Bmatrix} \bar{\mathbf{u}} \\ \bar{P}^w \\ \bar{T} \end{Bmatrix} + \begin{bmatrix} \mathbf{K}_T & -\mathbf{Q} & \mathbf{K}_{tT} \\ \mathbf{Q}^T & \mathbf{S} & \mathbf{R} \\ 0 & 0 & \mathbf{C}_t \end{bmatrix}$$

$$\frac{\partial}{\partial t} \begin{Bmatrix} \bar{\mathbf{u}} \\ \bar{P}^w \\ \bar{T} \end{Bmatrix} = \begin{Bmatrix} \frac{\partial \mathbf{f}^u}{\partial t} \\ \mathbf{f}^p \\ \mathbf{f}^t \end{Bmatrix}, \tag{10}$$

where $\bar{\mathbf{u}}$, $\bar{P}^w$, and $\bar{T}$ are the nodal values of the unknowns. $\mathbf{K}_T$ is tangential stiffness matrix, $\mathbf{Q}$ the matrix coupling the motion and flow equations, $\mathbf{Q}^T$ transposed of $\mathbf{Q}$, $\mathbf{K}_{tT}$ the tangential stiffness matrix of thermal loading, $\mathbf{H}$ permeability matrix, $\mathbf{S}$ compressibility matrix, $\mathbf{R}$ the matrix defining the flow induced by thermal loading, $\mathbf{K}_t$ the matrix including advection and conduction effects, $\mathbf{C}_t$ heat capacity matrix, and $\mathbf{f}^u$, $\mathbf{f}^p$ and $\mathbf{f}^t$ the vectors that include the effects of body forces, external loads, and fluid and heat fluxes.

3. Thermoplastic constitutive models

3.1. Abuel-Naga et al. Model [10]

The first thermoplastic model employed in this study has been developed by Abuel-Naga et al. [10] under the framework of critical state soil mechanics and modified Cam-clay model. An earlier version of this model was proposed by Abuel-Naga et al. [13] for isotropic condition. Then, this model was extended to the triaxial stress state by Abuel-Naga et al. [10]. This model was utilized in this study to simulate the stress-strain behavior of saturated clay under non-isothermal condition. This model is able to simulate thermal distortional and rotational kinematic hardening rule in addition to the conventional isotropic hardening rule. It uses temperature-dependent non-associated flow rule. In this model, slope of the swelling line and shear modulus are temperature independent, therefore, elastic behavior is not temperature-dependent.

Yield surface of this model has one more parameter than the conventional modified Cam-clay model. This additional parameter, α, is referred to as the fabric parameter and is used to express the temperature-dependency of the yield surface. Yield surface equation of this model is defined as follow:

$$\frac{P}{P_c} = \frac{M^2 + \alpha^2}{M^2 + (\eta^2 - \alpha^2)}, \tag{11}$$

where P_c is pre-consolidation effective stress, M the slope of Critical State Line (CSL) in the deviatoric plane $(q - p)$, and η is stress ratio $(\delta q/\delta p)$. It should be noted that the conventional modified Cam-clay yield surface equation can be obtained if $\alpha = 0$. As yield surface equation shows, thermal load induces a combined distortional and rotational hardening to the yield surface in addition to the classical critical state hardening relation of P_c due to mechanical loading. The fabric parameter α can be determined by model calibration against experimental data. Experimental results [14] show that the fabric parameter α increases as the soil temperature increases. The variation of fabric parameter α is expressed using a simple linear relation as follow:

$$\alpha(T) = \alpha(T_0) + c\left(\frac{T}{T_0} - 1\right), \tag{12}$$

where $\alpha(T_0)$ and $\alpha(T)$ are fabric parameters at the reference temperature (T_0) and elevated temperature (T), respectively. The parameter c is a dimensionless model constant which controls thermal evolution of α and can be determined by curve-fitting method.

A temperature-dependent non-associated flow rule has been adopted in this model. The temperature-dependent formula used for predicting incremental plastic strain ratio at different stress ratios (η) is:

$$\psi = \frac{d\varepsilon_v^p}{d\varepsilon_s^p} = -\beta \mathrm{Ln}\left(\frac{\eta}{M}\right), \tag{13}$$

where β is a soil parameter which expresses the effects of temperature on plastic strain increment ratio. The parameter β can be determined by tracing the variation of plastic strain increment ratio versus stress ratio. The experimental results [14] show that the fabric parameter β increases as the soil temperature increases. Thermal variation of β is expressed using a simple linear relation:

$$\beta(T) = \beta(T_0) + b\left(\frac{T}{T_0} - 1\right), \tag{14}$$

where $\beta(T_0)$ and $\beta(T)$ are the soil parameters at reference temperature (T_0) and elevated temperature (T), respectively. The parameter b is a dimensionless model constant that controls thermal evolution of β and can be determined by curve-fitting method.

In order to implement the proposed model in PISA software, it is necessary to extract the potential function from Eq. (14). In this process, an equation should be integrated to obtain the potential function; however, integrating this equation could not be accomplished mathematically. Therefore, the flow rule is replaced by the following equation which is similar to that of Cam-clay model and depends on temperature, using parameter β:

$$\psi = \frac{d\varepsilon_v^p}{d\varepsilon_s^p} = \beta \frac{M^2 - \eta^2}{2\eta}. \quad (15)$$

The results obtained from Eqs. (13) and (14) are almost equal. However, there are low differences in small values of η which is acceptable.

3.2. Hamidi and Khazaei Model [11]

The second model used in this study is Hamidi and Khazaei Model [11]. This model is also a thermal extension of the modified Cam-clay model and is able to simulate the thermo-mechanical behavior of saturated clays in triaxial stress condition at elevated temperatures higher than the ambient one up to 100°C. This model has six extra parameters χ, n, C, D, a and b than modified Cam-clay model which describe the variation of various soil properties with temperature. The main aspect of this model is thermal-dependency of both elastic and plastic states. In the following, a brief description of the model formulation has been presented. More details can be found in [11].

In order to consider the reduction in slope of NCL at elevated temperatures, the void ratio in this model is defined according to the following equation:

$$e_T = e_0 - \Delta e_{\max} \left(\frac{p'_0}{p'}\right)^n \left\{1 - \exp\left[\chi\left(1 - \frac{T}{T_0}\right)\right]\right\}, \quad (16)$$

where T_0 and T are the ambient and elevated temperatures, respectively; e_T and e_0 are void ratios of soil at elevated and ambient temperatures, respectively; χ and n are the model parameters which can be determined by plotting the variation of void ratio versus temperature and fitting the above equation; p'_0 and p' are initial and current mean effective stresses, respectively; $\Delta e_{\max}$ is the difference between void ratios of NCL and CSL in ambient temperature at the start of the test.

The elastic volumetric strain can be obtained by the following relation:

$$d\varepsilon_v^e = \frac{1}{K} dp' = \frac{k_T}{v_0} \frac{dp'}{p'}, \quad (17)$$

where K is elastic bulk modulus, v_0 initial specific volume ($v_0 = 1 + e_0$), and k_T the slope of unloading-reloading line at elevated temperature. Dependency of k_T to temperature is considered according to the following equation:

$$\frac{k_T}{k_0} = 1 + C \ln\left(\frac{T}{T_0}\right), \quad (18)$$

where k_0 is the slope of unloading-reloading line at ambient temperature. Also C is a model parameter for considering the change in slope of unloading-reloading line with temperature which should be determined according to the experimental data. According to the above equation, elastic bulk modulus is dependent on temperature and stress level. The stress-dependency of the Elastic bulk modulus is defined by the following equation:

$$K = K_0 \left(\frac{p'}{p'_0}\right)^a, \quad (19)$$

K_0 is bulk modulus at the mean effective stress of p'_0; a is a model parameter which describes non-linear dependency of elastic bulk modulus to the stress level.

Shear modulus is assumed to be both temperature- and stress-dependent according to Eq. (20):

$$G = G_0 \left(\frac{p'}{p'_0}\right)^b \left[1 + D \ln\left(\frac{T}{T_0}\right)\right], \quad (20)$$

where, G_0 is shear modulus relevant to the condition of ambient temperature and initial mean effective stress of p'_0. Also, D and b are model parameters that can be determined by curve-fitting to the experimental measurements of the variation of shear modulus versus temperature in different stress levels.

The plastic volumetric strain is considered temperature-dependent as follows:

$$d\varepsilon_v^p = \frac{\lambda_0 - k_T}{1+e} \frac{dp'_c}{p'_c} - n\Delta e_T \left(1 + \frac{\eta}{M-\eta}\right) \frac{dp'_c}{(1+e)p'_c}, \quad (21)$$

where λ_0 is the slope of isotropic consolidation line at ambient temperature, η the stress ratio, M the slope of critical state line, and p'_c preconsolidation pressure.

In this model, temperature-dependent associated flow rule is introduced by the following equation:

$$\psi = \frac{d\varepsilon_v^p}{d\varepsilon_s^p} = \frac{M^2 - \eta^2}{2\theta_T \eta}. \quad (22)$$

Yield surface is also temperature-dependent and has the following form:

$$q = \frac{p'M}{\sqrt{2\theta_T - 1}} \left[\left(\frac{p'_c}{p'}\right)^{\frac{2\theta_T - 1}{\theta_T}} - 1\right]^{0.5}, \quad (23)$$

where θ_T is a function of temperature. More details can be found in [11].

4. Numerical simulation

In order to simulate the THM response of saturated soils, geotechnical finite element program PISA has been used in this study. The first version of this code was developed at university of Alberta (named 'SAGE') [15]. Later, the formulation of this program was modified for analyzing THM problems [12]. In the modified version, saturated soil is modeled as a two-phase material based on the Biot's theory. Because of the important effects of temperature on stress-strain behavior of soils, thermoplastic constitutive models proposed by Abuel-Naga et al. [10] and Hamidi and Khazaei [11] have been implemented in PISA in the course of this study. The developed numerical model was used to simulate ATLAS experiment.

4.1. ATLAS experiment

A large-scale in situ experiment, called Admissible Thermal Loading for Argillaceous Storage (ATLAS), was designed as a part of the Interclay II program (1990-1994). A layout of this in situ test is shown in Figure 1. This experiment was performed in the HADES underground research facility (URF). The HADES-URF was built in Mol at the depth of 223 m in Boom clay formation. The ATLAS experiment comprises a horizontal main borehole (19 m long) with 4 heaters and 2 parallel instrumentation boreholes (16 m long) drilled at the distances of 1.184 m and 1.515 m from the main borehole. It includes two heating phases and a cooling phase. The first heating phase, started at a power of 900 W, provided by two of the four heaters and lasted nearly 3 years [8]. In this study, the first phase of heating has been simulated.

4.2. Boom clay

Underground research facility HADES was constructed in the middle of Boom clay formation at 223 m depth in Mol. Boom clay formation is almost horizontal and there are some sand layers above and below it that can bear water in. Underground water level is situated more or less at the ground surface. More details of this experiment can be found in [16].

Total vertical stress and pore water pressure at the level of HADES gallery are almost 4.5 and 2.025 MPa, respectively. K_0 value (ratio of horizontal to vertical effective stresses) was determined by laboratory methods and in-situ investigations. Results show that the vertical and horizontal stresses can be considered equal. Ambient temperature in HADES is about 16.5°C [16]. Basic physical, hydraulic, and thermal properties of Boom clay are listed in Table 1. The

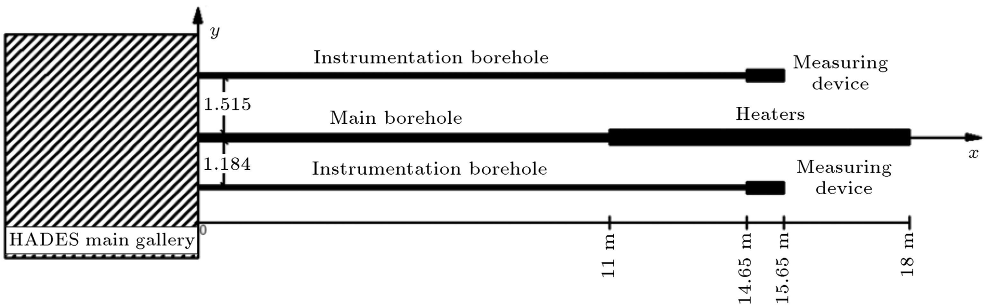

Figure 1. Schematic view of ATLAS experiment [17].

Table 1. Hydraulic, thermal, and physical characteristics of Boom clay.

Physical	Solid density	ρ_s	2670	(kg/m^3)
	Water density	ρ_w	1000	(kg/m^3)
	Water content	W	22-27	(%)
	Plastic limit	W_p	23-29	(%)
	Liquid limit	W_L	55-80	(%)
	Plasticity index	I_p	32-51	(%)
Hydraulic	Porosity	n	0.39	(-)
	Vertical permeability	k_v	2×10^{-19}	(m^2)
	Horizontal permeability	k_H	2×10^{-19}	(m^2)
	Water bulk modulus	K_w	2.2×10^{-6}	(kPa)
	Dynamic viscosity	μ	0.001	(Pa.s)
Thermal	Thermal conductivity of water	λ_w	0.57	(Wm^{-1}°C^{-1})
	Specific heat capacity of soil	$C_{p,s}$	732	(Jkg^{-1}°C^{-1})
	Specific heat capacity of water	$C_{p,w}$	4186	(Jkg^{-1}°C^{-1})
	Thermal dilation coefficient of solid	β_s	1.3×10^{-5}	(°C^{-1})
	Thermal dilation coefficient of water	β_w	3.5×10^{-4}	(°C^{-1})

Table 2. Mechanical parameters of Boom caly [16-20].

General	Friction angle	φ	18°
	Cohesion	c	$\approx$ 0.3 MPa
	Drained Young's modulus	E	0.3 MPa
	Preconsolidation pressure	$\mathbf{p'}_0$	6 MPa
	Overconsolidation ratio	OCR	2.64
	Slope of the swelling line	k	0.03
	Slope of the normal consolidation line	λ	0.14
	Poisson ratio	v	0.4
	Slope of critical state line	M	0.87
Abuel-Naga et al. Model	$\alpha(T_o)$		0.05
	$\beta(T_o)$		1.5
	c		0.107
	b		0.534
Hamidi and Khazaei Model	n		0.083
	$\Delta e_{\max}$		0.156
	χ		0.187
	D		-0.46
	C		-0.089
	b		1.3
	a		1.3

mechanical parameters used for numerical simulation of ATLAS experiment are presented in Table 2. As can be seen in this table, general mechanical parameters of Boom clay have been chosen based on the reported values by other investigators [16-19]. The constants of Abuel-Naga et al. and Hamidi and Khazaei Models, which are related to the thermal part of the models, have been calibrated in this study. For this purpose, laboratory tests performed on Boom clay by Delage et al. [19] and Cui et al. [20] were used. In these experimental studies, thermal consolidation tests and high-pressure triaxial tests at controlled temperatures have been carried out on Boom clay, respectively.

4.3. Main Aspects of modeling

The soil layers at the level of HADES gallery are homogenously Boom clay. Because of the great depth, the properties and stress state of soil layers can be considered isotropic [16,17]. In this regard, an axisymmetric analysis was performed. The axis of main borehole was assumed as the axis of symmetry. Eight-node rectangular elements were used in numerical analysis. The elements have four degrees of freedom at corner nodes (two solid phase displacements, a pore pressure, a temperature) and two degrees of freedom at middle nodes (two displacements). Aboustit [21] showed that using rectangular 8-node elements for displacement and rectangular 4-node elements for pore water pressure and temperature can reduce coupled analysis oscillation.

The simulation of ATLAS experiment was done in one-dimensional and two-dimensional cases. In the first case, a section in the middle of the heaters, perpendicular to ATLAS main borehole, was considered. For this "one-dimensional axisymmetric" domain, it was assumed that thermal and hydraulic fluxes propagation is only possible in radial direction. In other words, dissipation of pore water pressure and temperature is restricted in the axial direction (i.e. in the direction of the main borehole). This assumption makes the simulation less precise but decreases the time of computation. This approach is useful for pre-estimating the simulation. The internal boundary is permeable and displacement is restricted in X and Y directions at this boundary. At the external boundary, pore water pressure and temperature are kept at their initial values (2.025 MPa and 16.5°C) and displacement is restricted in both directions. Two other boundaries are impermeable and adiabatic, and displacement is restricted in perpendicular direction up to these boundaries. The finite element mesh used in this case is shown in Figure 2(a) which includes 41 elements and 208 nodes.

In the second geometry, the section of medium has been extended in the axial direction. Modeled domain is a region between internal boundary (coin-

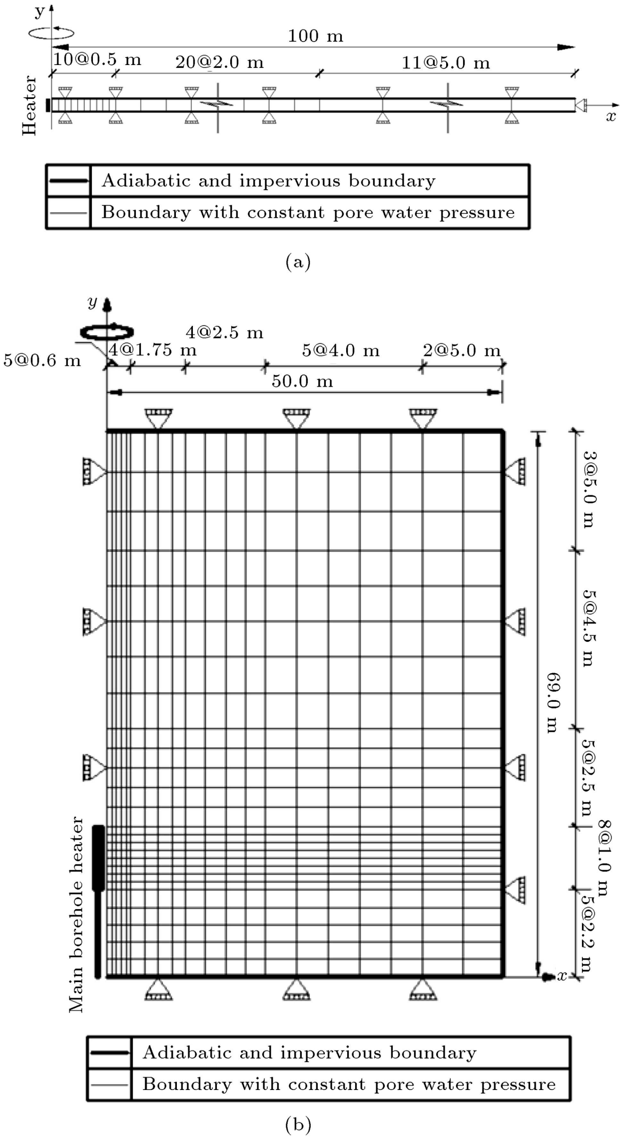

Figure 2. Finite element mesh: (a) one-dimensional axisymmetric mesh; and (b) two-dimensional axisymmetric mesh.

cided exactly with the external radius of the main borehole) and an external assumptive boundary. The bottom boundary is perpendicular to the main borehole and coincides with the HADES main gallery. For this "two-dimensional axisymmetric" case, propagation of thermal and hydraulic flows is considered both in axial and radial directions. Because of symmetric conditions, internal boundary is impermeable and adiabatic everywhere except along the heaters. In other boundaries, pore water pressure and temperature are kept at their initial values. Displacements in the normal direction to each boundary are restricted. Considered domains are 50 m and 69 m in radial and axial directions, respectively. Finite element mesh of this case is shown in Figure 2(b) which includes 520 elements and 1653 nodes.

5. Results of simulations and discussion

5.1. "Two-dimensional axisymmetric" simulation

Predicted and measured results of temperature are presented in Figure 3 in distances of 1.184 m and 1.515 m from heat source. Temperature increases rapidly during the first 50 days and then reaches a stable condition. In the vicinity of the heat source, temperature increase rate is higher and greater temperature is induced. This phenomenon was simulated accurately using Abuel-Naga et al. Model. However, Hamidi and Khazaei Model predicts quite identical temperature variations at different distances from the heat source which are not compatible with the experimental measurements.

Predicted and measured results of pore pressure are presented in Figure 4 in distances of 1.184 m and 1.515 m from heat source. The rate of pore water pressure variation is dependent on the temperature variation. At the beginning of heating process, when temperature increases rapidly, the rate of pore pressure increase is also high. When temperature reaches its peak value, dissipation of pore water pressure is more than the temperature-induced pore pressure, and consequently, its amount decreases. Dissipation of pore water pressure has been predicted accurately in this case. Getting away from the heat source, excess pore water pressure and its increasing rate reduce. In elastic analysis, lower excess pore water pressure than that in the thermoplastic case is developed and better agreement has been obtained by thermoplastic analysis.

Figure 5 shows the predicted results for radial displacement considering thermo-plastic and elastic behavior of the soil. There is no experimental measurement for radial displacement and the results were compared with Francois et al.'s [17] simulation results. At the start of heating, when the temperature increases rapidly in the soil mass, radial displacements increase due to the soil expansion. At the middle of heating, when the temperature reaches a steady state condition, compression of soil, due to the dissipation of pore water pressure, is more than soil expansion and the soil is compressed. Increase and subsequent decrease of radial displacement due to expansion and compression of soil mass was accurately simulated using Abuel-Naga et al. Model. However, using the Hamidi and Khazaei Model, only the increase of radial displacement was simulated and the subsequent decrease was not produced. In comparison with the results of simulation performed by Francois et al. [17], as shown in Figure 5, although a different constitutive model was utilized [17], good agreement is observed with the predictions of Abuel-Naga et al. Model and the main features have been simulated by these two different simulations.

For better understanding of thermo-hydro-mecha-

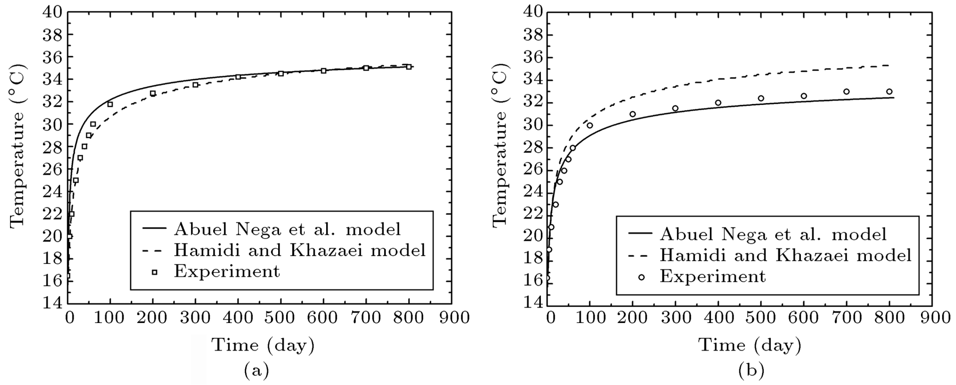

Figure 3. Time history of temperature variation in two-dimensional simulation: (a) At the distance of 1.184 m; and (b) at the distance of 1.515 m.

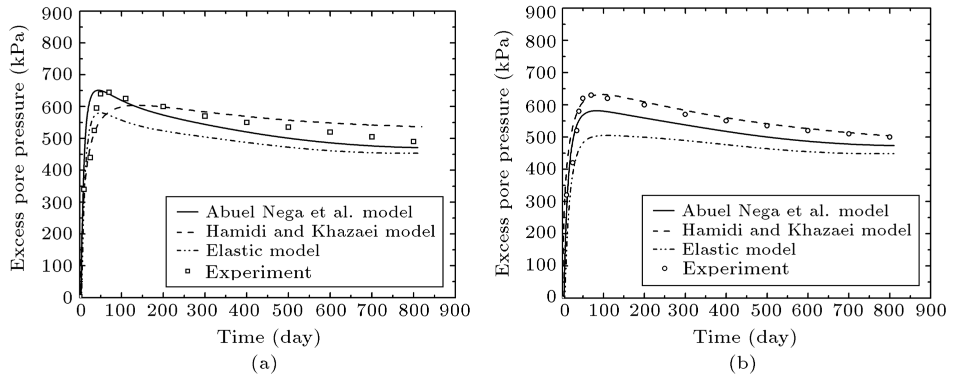

Figure 4. Time history of pore water pressure variation in two-dimensional simulation: (a) At the distance of 1.184 m; and (b) at the distance of 1.515 m.

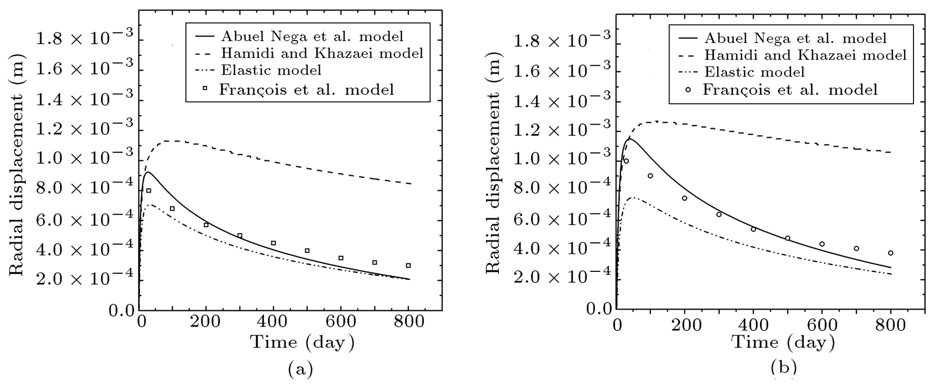

Figure 5. Time history of radial displacement in two-dimensional simulation: (a) At the distance of 1.184 m; and (b) at the distance of 1.515 m.

nical response of saturated clays, time history of pore water pressure and radial displacements have been determined using Abuel-Naga et al. Model at different distances from the heat source and the results are plotted in Figure 6. As this figure shows, getting away from the heat source, the peak and the rate of pore water pressure variations are reduced. However, an inverse trend is observed for the radial displacement results. The obtained radial displacements indicate a temperature-induced dilation behavior of the soil in the vicinity of heat source.

Figure 7 indicates the variation of computed temperature and pore pressure using Abuel-Naga et al. Model with distance from the heat source at different time intervals. As this figure shows, heat transfer occurs very slowly and its effects after 800 days are only distinguished up to 25 m from the heat source.

5.2. *"One-dimensional axisymmetric" simulation*

To study the effect of geometry on simulation results, the ATLAS experiment has been modeled in

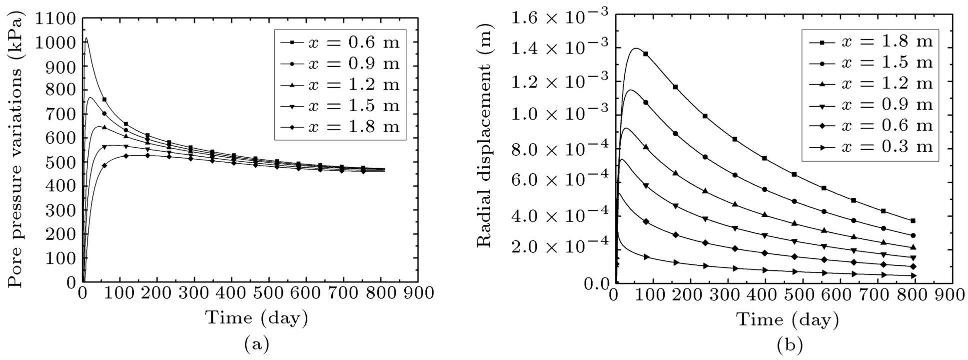

Figure 6. Time history of (a) pore water pressure, and (b) radial displacement using Abuel-Naga et al. Model at different distances from the heat source.

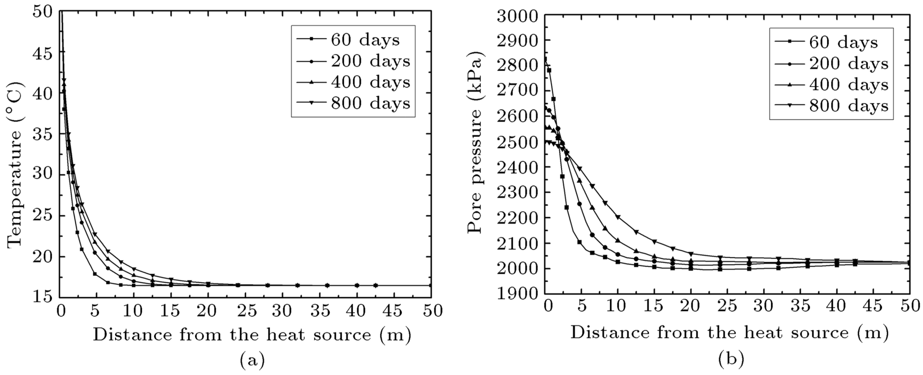

Figure 7. Variation of (a) temperature and (b) pore water pressure using Abuel-Naga et al. Model with a distance from the heat source at different times.

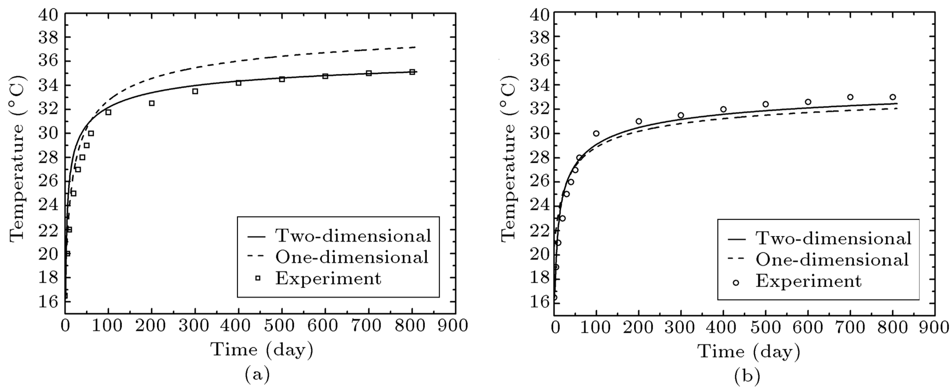

Figure 8. Time history of temperature variation in one-dimensional simulation: (a) At the distance of 1.184 m; and (b) at the distance of 1.515 m.

the one-dimensional case. Two-dimensional modeling indicates that THM phenomenon was simulated more accurately using Abuel-Naga et al. Model. So, this model has been used to simulate the one-dimensional case. In Figure 8, predicted and measured results of temperature variation at the distances of 1.184 m and 1.515 m from the axis of symmetry (at the level of two instrumentation boreholes) have been compared. Results of temperature variation are similar to the two-dimensional simulation. However, the agreement of predicted results with experimental measurements is better in the two-dimensional model.

Results of simulation for pore water pressure are compared with their measured values in Figure 9. When the rate of temperature variation is high, increase rate of pore water pressure is more. In closer areas to the heat source, more excess pore water pressure is developed and so, more hydraulic gradient is produced. Consequently, dissipation rate of pore water pressure is greater and there is a peak point in pore water pressure variation at a distance of 1.184 m from the heat source. Although the obtained results from one-dimensional modeling are almost acceptable, dissipation of the pore water pressure is not simulated

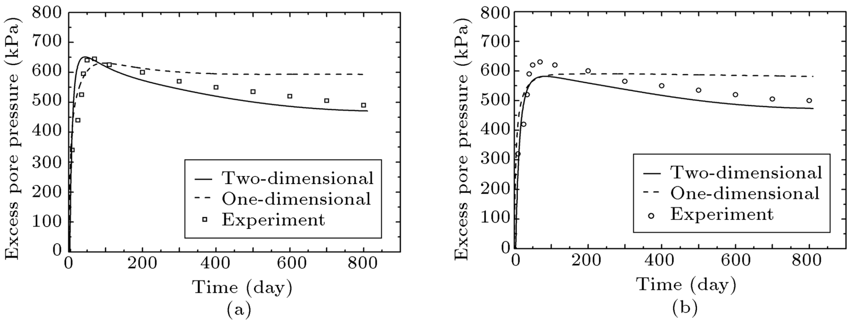

Figure 9. Time history of excess pore water pressure variation in one-dimensional simulation: (a) At the distance of 1.184 m; and (b) at the distance of 1.515 m.

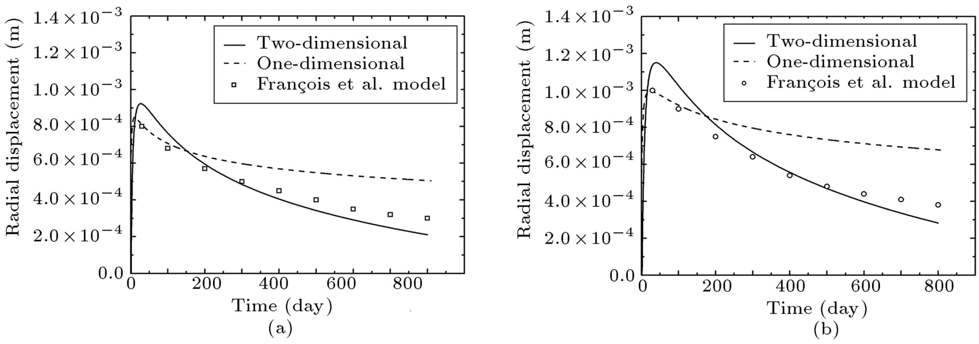

Figure 10. Time history of radial displacement in one-dimensional simulation: (a) At the distance of 1.184 m; and (b) at the distance of 1.515 m.

well. The reason could be explained by the restriction of diffusive process in the axial direction for this case. However it can be well simulated in two-dimensional analysis.

The above discussion for the results of radial displacement can be seen in Figure 10. Thus, it can be concluded that the two-dimensional modeling predicts more accurate results, especially for pore pressure and displacements.

5.3. Sensitivity analysis

Error in measuring the soil parameters are one of the main reasons for inconsistency between simulation and experimental results. Sensitivity analysis was performed on different thermal, hydraulic, and mechanical parameters using Abuel-Naga et al. Model. The results of sensitivity analysis show that some of the parameters have more influences on the simulation results which have been presented here.

Figure 11(a) shows the results of pore water pressure variations in the distance of 1.5 m from the heat source with different values of fluid compressibility. Existence of little gas bubbles in fluid increases it 10 to 100 times in compressibility. Any change in the compressibility of pore fluid reduces the excess pore water pressure 2 to 3 times. Figure 11(b) indicates pore water pressure variations for three different values of soil permeability. When permeability is high, the role of advection in heat transfer increases. In this state, the governing process in heat transfer is advection. Therefore, the reach time to the maximum value of pore water pressure is less. On the other hand, because of the rapid dissipation in pore water pressure, the maximum value of pore water pressure will decrease.

In Figure 11(c), pore water pressure variations have been shown for three different values of fluid thermal expansion coefficient. As the fluid thermal expansion coefficient increases, the differential volume changes of fluid and soils increase which results in the increase in excess pore water pressure.

In Figure 11(d), pore water pressure variations have been presented for different values of the thermal conductivity coefficient. When permeability is low, the role of advection in heat transfer can be ignored and the governing process in heat transfer is conduction. Therefore, increase in thermal conductivity coefficient increases heat transfer and pore water pressure development in the soil.

In Figure 12, the obtained radial displacements have been shown for three various values of fluid thermal expansion coefficient and soil permeability. Increase in fluid thermal expansion coefficient results in the increase in excess pore water pressure. Consequently, the effective stress decreases and displacement increases. The effect of permeability variation on displacement is the same as its effect on pore water pressure as described above.

Figure 13 indicates radial displacement and tem-

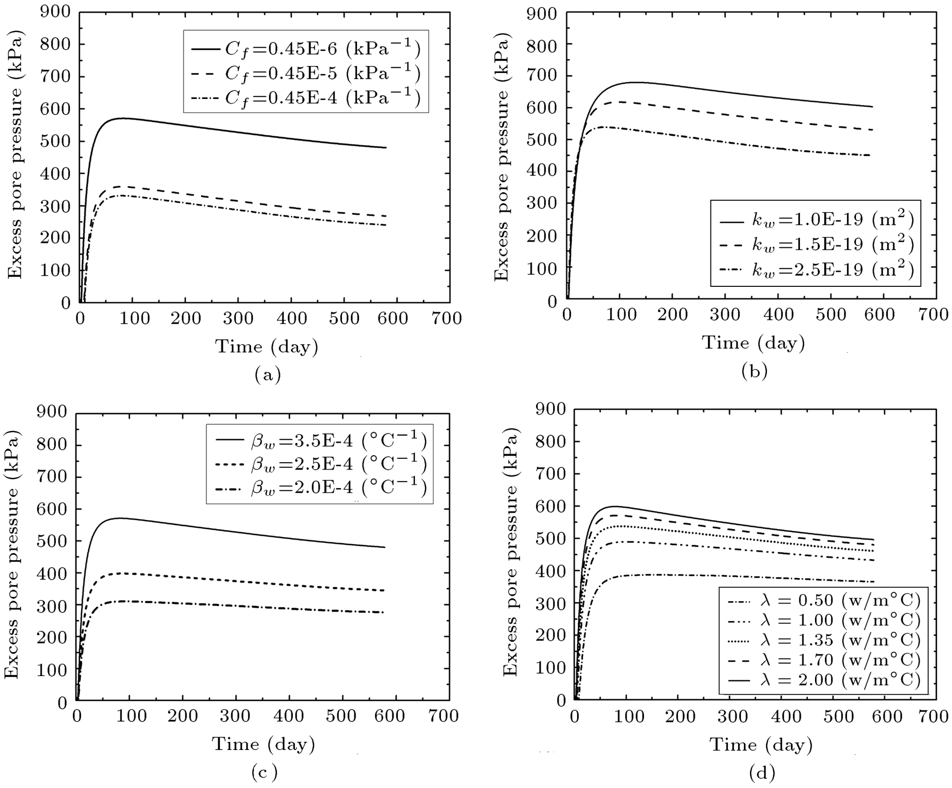

Figure 11. Time history of pore water pressure for different values of (a) fluid compressibility, (b) soil permeability, (c) fluid expansion coefficient, and (d) thermal conductivity coefficient.

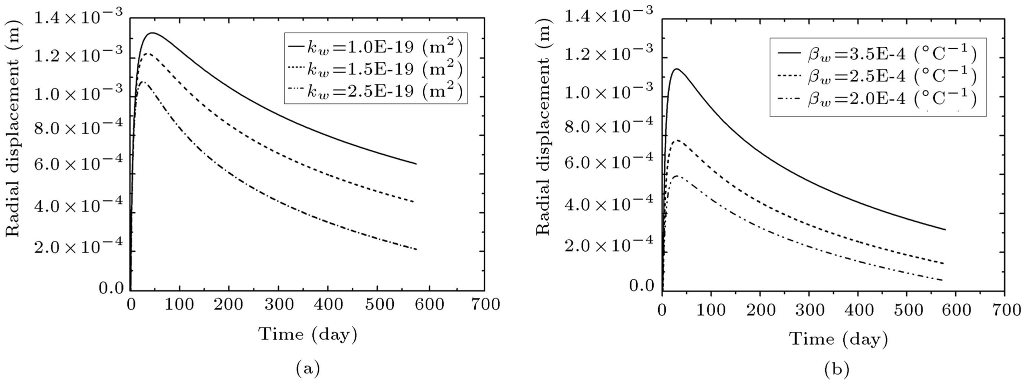

Figure 12. Time history of radial displacement for different values of (a) soil permeability, and (b) fluid expansion coefficient.

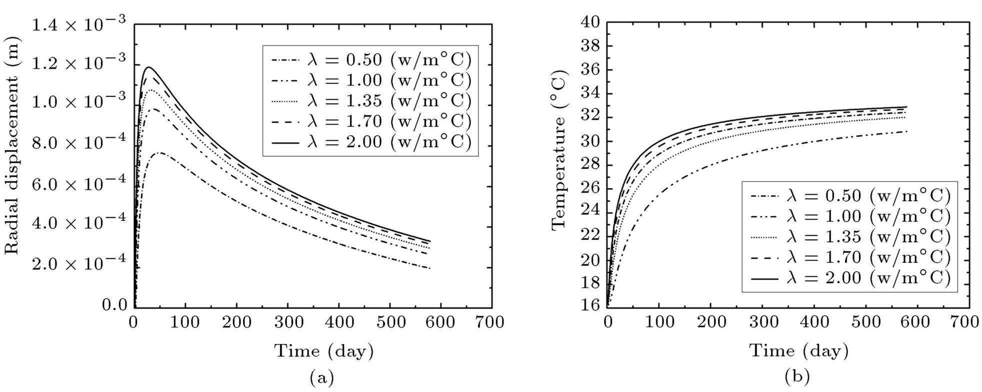

Figure 13. Time history of radial displacement and temperature for different values of thermal conductivity coefficient.

perature variations for different values of thermal conductivity coefficient. Due to the low permeability, the governing process of heat transfer is conduction. Therefore, heat transfer and consequent displacements increase with increase in the thermal conductivity coefficient.

6. Conclusion

Because of the significant effects of heating on the mechanical behavior of clays, using the temperature-dependent (thermo-mechanical) constitutive model in THM analysis leads to more accurate results. In this research, coupled thermo-hydro-mechanical processes, which occur in the saturated soil mass as a result of thermal loading, were analyzed employing two different thermo-plastic constitutive models. Abuel Naga et al. Model is able to simulate thermal distortional and rotational kinematic hardening rule in addition to the conventional isotropic hardening rule. Also, it is able to take temperature effects into consideration on the incremental plastic strain ratio. However, the effects of temperature on the elastic behavior are not considered in this model. Thermal behavior of soil in both elastic and plastic states can be modeled by Hamidi and Khazaei Model. The basis of this model is on the movement of Normal Consolidation Line (NCL) to lower values of void ratio at elevated temperatures.

ATLAS large scale in-situ experiment which simulates heat generation in soil was simulated using the developed numerical model. Comparison between predictions and measurements reveals that the employed models can capture the main aspects of the THM behavior of saturated clays. However, radial displacements can be more accurately simulated using Abuel Naga et al. Model. Using the Hamidi and Khazaei Model, only the increase of radial displacement was simulated and the subsequent decrease was not produced. Also, the variations of temperature in the soil mass can be more accurately simulated using Abuel Naga et al. Model.

Simulation results reveal the need for a two-dimensional analysis for better estimation of pore water pressure and displacement values. Dissipation of pore water pressure is not simulated well in the one-dimensional case. The reason could be explained by the restriction of diffusive process in axial direction in this case. This reason is also correct for the results of radial displacement. However, this can be precisely simulated in two-dimensional analysis.

References

1. Chijimatsu, M., Fujita, T., Sugita, Y., Amemiya, K. and Kobayashi, A. "Field experiment, results and THM behavior in the Kamaishi mine experiment", *Int. J. Rock Mech. Min. Sci.*, **38**, pp. 67-78 (2001).

2. Rutqvist, J., Chijimatsu, M., Nguyen, T.S., Jing, L., Noorishad, J. and Tsang, C.F. "Coupled thermo-hydro-mechanical analysis of a heater test in fractured rock and bentonite at Kamaishi Mine", *Int. J. Rock Mech. Min. Sci.*, **38**, pp. 129-142 (2001).

3. Datta, R., Barr, D. and Boyle, W. "Measuring thermal, hydrological, mechanical, and chemical responses in the Yucca Mountain drift scale test", in Stephansson, O., Hudson, J.A., Jing, L., Eds., *Coupled Thermo-Hydro-Mechanical-Chemical Processes in Geo-System-Fundamentals, Modeling, Experiments and Applications*, Elsevier, Geo-Engineering Book Series, pp. 155-160, Oxford, UK (2004).

4. Rutqvist, J., Barr, D., Datta, R., Gens, A., Millard, A., Olivella, S., Tsang, C.F. and Tsang, Y. "Coupled thermal-hydrological-mechanical analysis of the Yucca mountain drift scale test-comparison of field measurements to prediction of four different numerical models", *Int. J. Rock Mech. Min. Sci.*, **42**, pp. 680-697 (2005).

5. Alonso, E., Alcoverro, J., Coste, F. et al. "The FEBEX benchmark test: Case definition and comparison of modeling approaches", *Int. J. Rock Mech. Min. Sci.*, **45**(5-6), pp. 611-38 (2005).

6. Gens, A., Garcia-Molina, A.J., Olivella, S., Alonso, E.E. and Huertas, F. "Analysis of full scale in situ test simulating repository conditions", *Int. J. Numer. Anal. Methods Geomech.*, pp. 22:515-548 (1998).

7. Hoxha, D., Jiang, Z., Homand, F., Giraud, A., Su, K. and Wileveau, Y. "Impact of THM constitutive behavior on the rock-mass response: case of HE-D experiment in mont-terri underground rock laboratory", In *EUROCK 2006 Multiphysics Coupling and Long Term Behaviour in Rock Mechanics*, pp. 199-204 (2006).

8. De Bruyn, D. and Labat, S. "The second phase of ATLAS: The continuation of a running THM test in the HADES underground research facility at Mol", *J. Eng. Geol.*, **64**, pp. 309-316 (2002).

9. Lewis, R.W. and Schrefler, B.A., *The Finite Element Method in the Static and Dynamic Deformation and Consolidation of Porous Media*, John Wiley, Chichester, Second Edn. (1998).

10. Abuel-Naga, H.M., Bergado, D.T., Bouazza, A. and Pender, M. "Thermomechanical model for saturated clays", *J. Géotechnique*, **59**(3), pp. 273-278 (2009).

11. Hamidi, A. and Khazaei, S. "A thermomechanical model for saturated clays", *Int. J. Geotech. Eng.*, **4**(4), pp. 445-459 (2010).

12. Pak, A. "Numerical modeling of hydraulic fracturing", Department of Civil and Environmental Engineering, PhD Thesis, University of Alberta (1997).

13. Abuel-Naga, H.M., Bergado, D.T., Bouazza, A. and Ramana, G.V. "Volume change behavior of saturated

clays under drained heating conditions: Experimental results and constitutive modeling", *Can. Geotech. J.*, **44**(8), pp. 942-956 (2007a).

14. Abuel-Naga, H.M., Bergado, D.T. and Lim, B.F. "Effect of temperature on shear strength and yielding behavior of soft Bangkok clay", *Soil Found*, **47**(3), pp. 423-436 (2007b).
15. Chan, D. and Morgenstern, N. "SAGE: A finite element program for stress analysis in geotechnical engineering", *Program User Manual, Geotechnical Group*, University of Alberta (1988).
16. Li, X., Bernier, F., Vietor, T. and Lebon, P. "Report of TIMODAZ project", European Commission (2007).
17. Francois, B., Laloui, L. and Laurent, C. "Thermo-hydro-mechanical simulation of ATLAS in situ large scale test in BOOM clay", *Comput. Geotech.*, **36**, pp. 626-640 (2009).
18. Sultan, N., Delage, P. and Cui, Y.J. "Temperature effects on the volume change behavior of Boom clay", *J. Eng. Geol.*, **64**, pp. 135-145 (2002).
19. Delage, P., Sultan, N. and Cui, Y.J. "On the thermal consolidation of Boom clay", *Can. Geotech. J.*, **37**(2), pp. 343-354 (2000).
20. Cui, Y.J., Le, T.T., Tang, A.M., Delage, P. and Li, X.L. "Investigating the time-dependent behavior of Boom clay under thermomechanical loading", *J. Géotechnique.*, **59**(4), pp. 319-329 (2009).
21. Aboustit, B.L., Advani, S.H. and Lee, J.K. "Vibrational principles and finite element simulations for thermo-elastic consolidation", *Int. J. Numer. Anal. Methods Geomech.*, **9**, pp. 49-69 (1985).

Biographies

Somayeh Delfan received her BSc degree in Civil Engineering from Mazandaran University, Babol, Iran, and her MSc degree in Environmental Engineering from Kharazmi University, Tehran, Iran. Her research interests are in numerical modeling of geo-environmental problems and coupled Thermo-Hydro-Mechanical phenomena. She is currently working as a design engineer at a geotechnical consultant company.

Hadi Shahir received his BSc degree in Civil Engineering from Sharif University of Technology, Tehran, Iran. He also received his MSc and PhD degrees in Geotechnical Engineering from Sharif University of Technology. Dr. Shahir is currently a Faculty Member and Assistant Professor of Geotechnical Engineering in Kharazmi University, Tehran, Iran. He involved in teaching and research in various fields of geotechnical engineering.

Amir Hamidi received his BSc degree in Civil Engineering from Sharif University of Technology, Tehran, Iran. He also received his MSc and PhD degrees in Geotechnical Engineering from Sharif University of Technology. Dr. Hamidi is currently a Faculty Member and Associate Professor of Geotechnical Engineering in Kharazmi University, Tehran, Iran. He involved in teaching and research in various fields of geotechnical engineering.

Elhameh Lotfi received her BSc degree in Civil Engineering from Mohaghegh Ardabili University, Ardabil, Iran, and her MSc degree in Environmental Engineering from Kharazmi University, Tehran, Iran. Her research interests are in numerical modeling of geo-environmental and especially coupled thermo-hydro-mechanical phenomena.